Distribution of detrital minerals and sediment color in western Arctic Ocean and northern Bering Sea sediments: Changes in the provenance of western Arctic Ocean sediments since the last glacial period

Daisuke Kobayashi [a, 1], Masanobu Yamamoto [a, b, *], Tomohisa Irino [a, b], Seung-Il Nam [c], Yu-Hyeon Park [a, 2], Naomi Harada [d], Kana Nagashima [d], Kazuhisa Chikita [e], Sei-Ichi Saitoh [f, g]

[a] Graduate School of Environmental Science, Hokkaido University, Kita-10, Nishi-5, Kita-ku, Sapporo, Japan
[b] Faculty of Environmental Earth Science, Hokkaido University, Kita-10, Nishi-5, Kita-ku, Sapporo, Japan
[c] Korea Polar Research Institute, 26 Songdomiraero, Yeonsu-gu, Incheon 21990, South Korea
[d] Research Institute for Global Change, Japan Agency for Marine-Earth Science and Technology, 2-15 Natsushimacho, Yokosuka 237-0061, Japan
[e] Faculty of Science, Hokkaido University, Kita-10, Nishi-8, Kita-ku, Sapporo, Japan
[f] Arctic Research Center, Hokkaido University, Kita-21, Nishi-11, Kita-ku, Sapporo, Japan
[g] Faculty of Fisheries Sciences, Hokkaido University, 3-1-1 Minatocho, Hakodate 041-8661, Japan

ARTICLE INFO

ABSTRACT

This paper describes the distribution of detrital minerals and sediment color in the surface sediments of the western Arctic Ocean and the northern Bering Sea and investigates the relationship between mineral composition and sediment provenance. This relationship was used to determine the provenance of western Arctic Ocean sediments deposited during the last glacial period. Sediment color is governed by water depth, diagenesis, and mineral composition. An a*−b* diagram was used to trace color change during diagenesis in the Arctic Ocean sediments. The mineral composition of surface sediments is governed by grain size and provenance. The feldspar/quartz ratio of the sediments studied was higher on the Siberian side than on the North American side of the western Arctic Ocean. The (chlorite + kaolinite)/ illite and chlorite/illite ratios were high in the Bering Sea but decrease northwards in the Chukchi Sea. Thus, these ratios are useful for provenance studies in the Chukchi Sea area as indices of the Beaufort Gyre circulation and the Bering Strait inflow. The sediments deposited during the last glacial period have a lower feldspar/quartz ratio and a higher dolomite intensity than Holocene sediments on the Chukchi Plateau, suggesting a greater contribution of North American grains during the last glacial period.

© 2016 Elsevier B.V. and NIPR. All rights reserved.

1. Introduction

Changes in the system of currents regulate the fate of sea ice in the Arctic Ocean, and are involved in the processes of global climate change via the ice-albedo feedback and the delivery of freshwater to the North Atlantic Ocean (Miller et al., 2010; Screen and Simmonds, 2010). The system of currents in the Arctic Ocean consists of the Beaufort Gyre (BG) and the Transpolar Drift (TPD), which are driven by surface winds (Proshutinsky and Johnson, 1997; Rigor et al., 2002). The Beaufort Sea exports much of its ice to the eastern Arctic Ocean via the BG. The TPD carries the sea ice from the eastern Arctic Ocean to the Atlantic via the Fram Strait. The Bering Strait inflow (BSI) is also an important element that transports heat and freshwater from the Bering Sea to the Chukchi Sea (e.g., Weingartner et al., 2005; Woodgate and Aagaard, 2005; Woodgate et al., 2005a,b; Shimada et al., 2006). Shimada et al. (2006) suggested that the inflow of warm Pacific water causes catastrophic changes in sea ice stability in the western Arctic Ocean.

The mineral composition of sediments has been used to reconstruct the ocean circulation, sea ice drift, and iceberg

* Corresponding author. Graduate School of Environmental Science, Hokkaido University, Kita-10, Nishi-5, Kita-ku, Sapporo, Japan.
E-mail address: myama@ees.hokudai.ac.jp (M. Yamamoto).
[1] Present address: Fujitsu Advanced Solutions, Co. Ltd., 1-2-4 Shinkoyasu, Kanagawa-ku, Yokohama 221-0013, Japan.
[2] Present address: Division of Earth Environmental System, Pusan National University, Busan 609−735, South Korea.

Table 1
Surface sediment samples.

Leg	Core	Latitude (°N)	Longitude (°E)	Water depth (m)	Location	Lithology
ARA03B	41	82.3200	171.5200	2758	Makarov basin	Clayey silt
ARA03B	18	79.0000	174.0000	2452	Makarov basin	Clayey silt
ARA03B	16	78.5000	−177.7500	1228	Arlis plateau	Clayey silt
ARA02B	06[a]	78.0055	−168.3589	453	Chukchi plateau	Clayey silt
ARA02B	09	77.9999	−179.3347	1577	Arlis plateau	Clayey silt
ARA02B	11	77.9997	173.9981	1596	East siberian slope	Clayey silt
ARA02B	08	77.9991	−175.6784	1375	Arlis plateau	Clayey silt
ARA03B	19	77.9700	173.0400	1091	East Siberian slope	Clayey silt
ARA03B	30	77.0800	−172.2900	2013	Chukchi Abyssal plain	Clayey silt
ARA03B	29	77.0100	−177.3600	1396	Arlis plateau	Clayey silt
ARA02B	15	76.4023	−179.3416	1803	Arlis plateau	Clayey silt
ARA02B	16A	76.3994	−176.2174	337	Chukchi Abyssal plain	Clayey silt
ARA02B	16B	76.3994	−176.2174	1073	Chukchi Abyssal plain	Clayey silt
ARA02B	18A	76.2885	−167.1604	435	Chukchi plateau	Clayey silt
ARA02B	18B	76.2885	−167.1604	406	Chukchi plateau	Clayey silt
ARA03B	28	76.2200	−179.8400	1179	Arlis plateau	Clayey silt
ARA02B	13[a]	76.0040	174.0003	340	East Siberian slope	Clayey silt
ARA01B	25	76.0008	−159.0007	820	Northwind ridge	Clayey silt
ARA01B	21	75.9981	−156.0156	920	Northwind ridge	Clayey silt
ARA01B	27	75.9695	−160.0028	2100	Northwind ridge	Clayey silt
ARA03B	27	75.5200	178.7800	678	East Siberian slope	Clayey silt
ARA01B	32	75.4963	−163.0149	1920	Northwind Abyssal plain	Clayey silt
ARA03B	26	75.3700	177.2900	354	Arlis plateau	Clayey silt
ARA02B	03B	75.1165	−166.3405	455	Chukchi plateau	Clayey silt
ARA02B	03A[a]	75.1079	−166.3405	423	Chukchi plateau	Clayey silt
ARA01B	13	75.0175	−156.0072	3900	Northwind ridge	Clayey silt
ARA01B	08	75.0006	−159.0005	1993	Northwind ridge	Clayey silt
ARA01B	05	74.9987	−159.0167	940	Northwind ridge	Clayey silt
ARA02B	02[a]	74.2989	−167.6520	320	Chukchi slope	Silt
ARA01B	04	73.7349	−167.0042	43	Chukchi shelf	clayey silt
ARA02B	01B	73.6343	−166.5065	119	Chukchi shelf	Silt
ARA02B	01A[a]	73.6314	−166.5183	123	Chukchi shelf	Silt
MR06	12EX	73.5998	−166.0007	53	Chukchi shelf	Sandy silt
ARA01B	03	73.5193	−166.0163	113	Chukchi shelf	Silt
ARA01B	01	73.1289	−168.0156	72.5	Chukchi shelf	Silt
MR06	12	72.4322	−166.9642	51	Chukchi shelf	Sandy silt
MR06	13	72.0007	−165.9995	46	Chukchi shelf	Sandy silt
MR06	14	70.9997	−165.9975	43	Chukchi shelf	Sandy silt
MR06	15	69.9998	−168.0002	48	Chukchi shelf	Sandy silt
MR00	15	69.7562	−138.1627	163	Mackenzie estuary	
MR06	16	68.5005	−167.9992	54	Chukchi shelf	Silty sand
MR06	17	66.9998	−166.9992	40	Chukchi shelf	Sandy silt
MR06	18	63.9998	−169.0030	35	Bering shelf	Sand
MR06	B52	63.9000	−166.2000		Bering shelf	
MR00	7	63.5017	−165.4998	21.3	Bering shelf	
MR06	19	63.0003	−167.4990	33	Bering shelf	Sand
OS	5	62.9600	−164.9200		Yukon estuary	Sand
OS	P2	62.8800	−165.0800		Yukon estuary	Sand
OS	1	62.8500	−164.9600		Yukon estuary	Sand
OS	P1	62.8400	−164.8800		Yukon estuary	Sand
MR06	22	62.0052	−176.0027	98	Bering shelf	Sandy silt
MR06	21	62.0007	−172.0005	56	Bering shelf	Silty sand
MR06	23	60.1587	−179.4633	1004	Bering slope	Silty sand
MR06	25	60.0748	−179.4632	1158	Bering slope	Silty sand
MR06	26	59.9997	−176.0000	132	Bering shelf	Sandy silt
MR06	30	58.5002	−172.0002	101	Bering shelf	Sandy silt
MR06	31	58.3832	−170.0007	74	Bering shelf	Silty sand
MR06	32	57.0003	−167.5005	77	Bering shelf	Sand

[a] Whole core analyzed (rather than just core top as for other samples).

discharge in the Arctic Ocean (e.g., Bischof et al., 1996; Bischof and Darby, 1997; Vogt, 1997). Spatial variation in mineral composition is found in Arctic shelf sediments. Accordingly, we can potentially identify the provenance of sediments by analyzing their mineral composition (e.g., Naidu et al., 1982; Naidu and Mowatt, 1983; Stein et al., 1994; Bischof et al., 1996; Vogt, 1997; Wahsner et al., 1999; Kalinenko, 2001; Stein, 2008; Ortiz et al., 2009; Darby et al., 2011; Nwaodua et al., 2014). Using the spatial variability of detrital minerals, the ocean circulation and ice drift patterns have been reconstructed to reveal late Pleistocene changes (Stein et al., 2010a,b), glacial–interglacial contrasts (Bischof and Darby, 1997;

Phillips and Grantz, 2001; Vogt et al., 2001; Darby and Bischof, 2002), and Holocene changes in the TPD and BG configuration (Darby and Bischof, 2004; Darby et al., 2012) and the Bering Strait inflow (Ortiz et al., 2009).

The Chukchi Sea is located in the region where the BSI meets the BG circulation. Thus, the Chukchi Sea and the adjacent seas are suitable areas in which to investigate the evolution of the BG circulation and the BSI. In the present study, we examined the distribution of detrital minerals in surface sediments from the western Arctic Ocean, the Bering Sea, and the Yukon and Mackenzie River estuaries with the aim of determining the relationship between
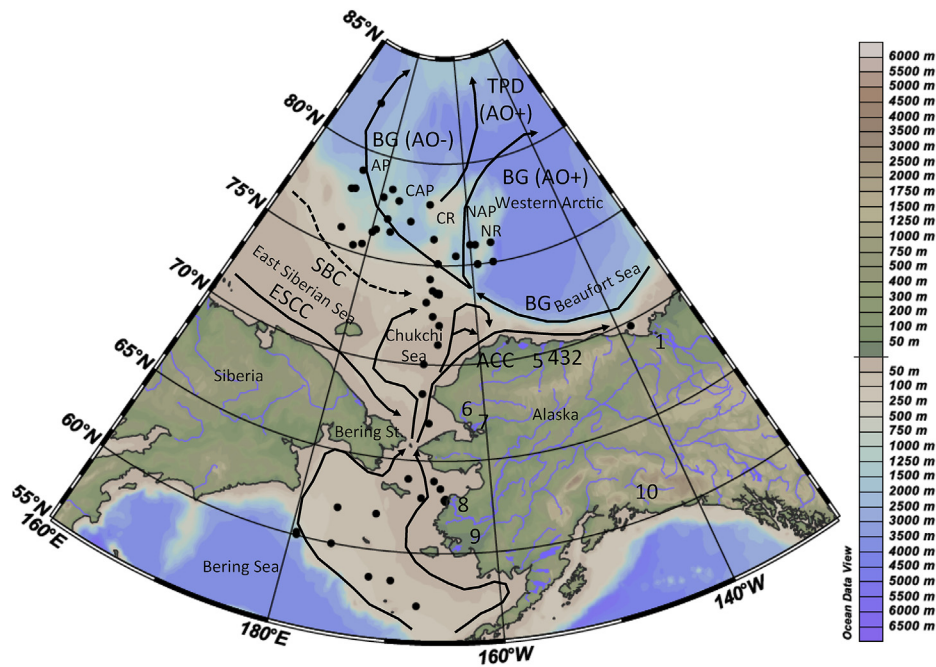
Fig. 1. Map showing the locations of surface sediment samples. BG: Beaufort Gyre. ACC: Alaskan Coastal Current. SBC: Subsurface Boundary Current. ESCC: East Siberian Coastal Current. TPD: Transpolar Drift. NR: Northwind Ridge. NAP: Northwind Abyssal Plain. CR: Chukchi Ridge. CAP: Chukchi Abyssal Plain. AP: Arlis Plateau. 1: Mackenzie River. 2: Canning River. 3: Sagavanirktok River. 4: Kuparuk River. 5: Colville River. 6: Noatak River. 7: Kobuk River. 8: Yukon River. 9: Kuskokwim River. 10: Copper River. AO+ and AO− indicate the paths of currents in the positive and negative phases of the Arctic Oscillation, respectively.

mineral composition and sediment provenance. We also examined changes in mineral composition in five short cores from the Chukchi Plateau, the Chukchi shelf, and the East Siberian slope to investigate changes in sediment provenance since the last glacial period.

Nagashima et al. (2012) and Park et al. (2014) analyzed the same sample set used in the present study, and showed that coarse sediments are distributed across the Yukon and Mackenzie River estuaries, the northern Bering Sea near Bering Strait, and some areas of the Bering Sea. In the western Arctic Ocean, silt dominates and becomes finer, from sandy silt to clayey silt, northwards. The dominance of coarse sediments in the inner shelf of the Chukchi and Bering seas is attributable to both coastal erosion and river discharge from small Alaskan and Siberian rivers, as well as the Yukon River, and also the selective removal of fine particles in high-energy environments. A gap exists in the grain size distribution of sediments between the areas south of 73.5°N and those areas north of 75°N in the Chukchi Sea, which corresponds to the average position of the seasonally minimum sea ice margin. In the area south of 73.5°N, well-sorted fine particles advected from the south by northward flowing currents are deposited in low-energy environments. The advection of fine particles is also suggested by the northward increasing trend of the $^{87}Sr/^{86}Sr$ ratio (Asahara et al., 2012). In the area north of 75°N, the sediments are a combination of well-sorted fine silt derived from the East Siberian shelf, inner Chukchi shelf, and the Alaskan margin deposited by currents, and very fine particles carried by sea ice drift from the North American margin via the BG circulation.

2. Samples and methods

2.1. Samples

In total, 58 core-top (0–0.5 or 0–1 cm depth) sediment samples were collected in the western Arctic Ocean from the Chukchi shelf,

the northern Chukchi slope, the Northwind Ridge, the Northwind Abyssal Plain, the Chukchi Plateau, the Chukchi Abyssal Plain, the Arlis Plateau, the East Siberian slope, the Makarov Basin, the Bering shelf and slope, and the Yukon and Mackenzie River estuaries, using multiple and box corers. These were obtained during the RV *Araon* cruises in 2010, 2011, and 2012 (ARA01B, ARA02B, and ARA03B, respectively), the RV *Mirai* cruises in 2000 and 2006 (MR00 and MR06 cruises, respectively), and the T/S *Oshoro-maru* cruise in 2009 (OS; Table 1 and Fig. 1).

Five short cores were retrieved using a multiple corer during the ARA02B cruise. Cores ARA02B 01A MUC (28 cm long), 02 MUC (35 cm long), 03A MUC (32 cm long), 06 MUC (32 cm long), and 13 MUC (25 cm long) were retrieved from the western Arctic Ocean (Table 1). The sediments of core 01A MUC, from the Chukchi shelf, consist of dusty yellowish-brown clayey silt (0–3 cm) and olive-gray clayey silt (3–28 cm). The sediments of core 02 MUC, from the Chukchi slope, consist of grayish-brown clayey silt (0–7 cm) and dark greenish-gray clayey silt (7–35 cm). The sediments of core 03A MUC, from the Chukchi Plateau, consist of grayish-brown clayey silt (0–23 cm) and olive-gray silt with dolomite dropstones (23–32 cm). The sediments of core 06 MUC, from the Chukchi Plateau, consist of dark yellowish-brown silt with dolomite fragments (0–14 cm) and light olive-brown silt with dolomite fragments (14–32 cm). The sediments of core 13 MUC, from the East Siberian slope, consist of dark yellowish-brown silt (0–11 cm), light yellowish-brown silt (11–15 cm), dark yellowish-brown silt (15–20 cm), light yellowish-brown silt (20–23 cm), and dark yellowish brown silt (23–24.5 cm). The cores were subsampled and stored in a freezer on board and then freeze-dried in the laboratory. The samples were powdered prior to analysis.

2.2. Methods

2.2.1. Color measurement

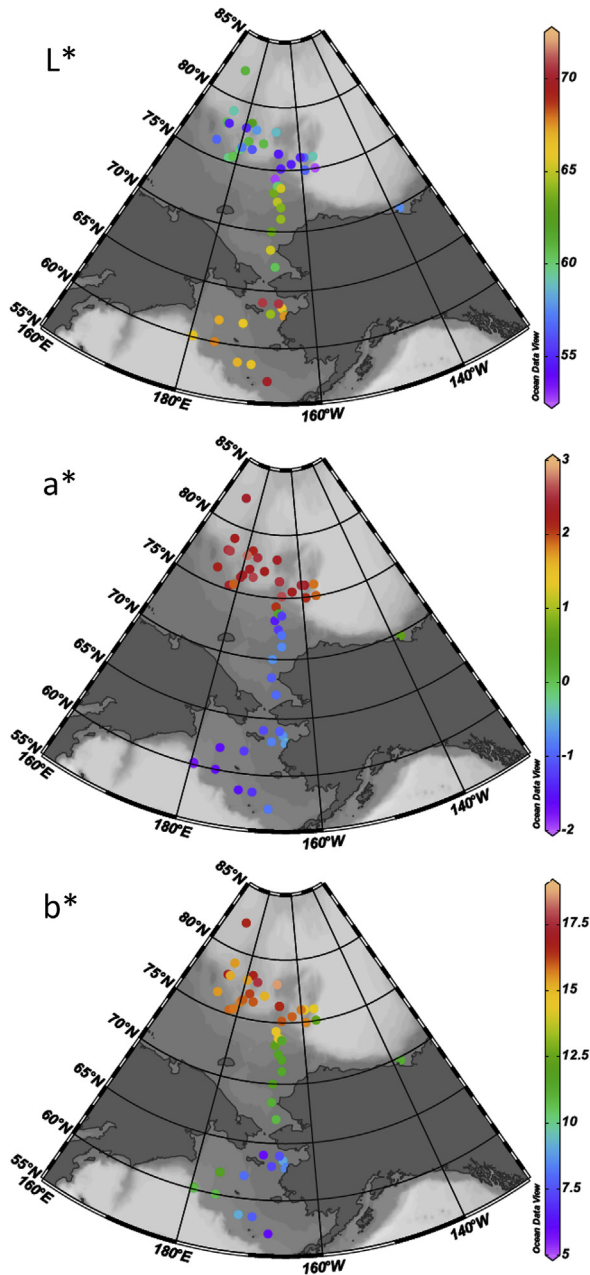The color of the dried and powdered sediment samples was

Fig. 2. Spatial distributions of color indices L*, a*, and b* for the surface sediments.

analyzed using a Konica Minolta CM-2002 ultraviolet/visible spectrometer (400−700 nm wavelength range; 10 nm resolution; 8 mm spot size). The results are shown as colorimetric indices; i.e., the sediment brightness (L*), the red−green contrast (a*), and the yellow−blue contrast (b*).

2.2.2. X-ray diffraction

Analysis of the mineral composition of the bulk sediments was conducted using a MAC Science MX-Labo X-ray diffractometer (XRD) equipped with a CuKα tube and monochromator. A tube voltage of 40 kV and current of 20 mA were used. The scanning speed was 4° 2θ/min and the data sampling step was 0.02° 2θ. Each powdered sample was mounted on a glass holder with a random orientation and X-rayed from 2 to 40° 2θ. In this study, the background-corrected diagnostic peak intensity was used to

determine the abundance of each mineral. The relative XRD intensities of illite including mica ("illite" hereafter) at 8.82° 2θ (d = 10.1 Å), hornblende at 10.4° 2θ (d = 8.5 Å), chlorite including kaolinite ("chlorite + kaolinite" hereafter) at 12.4° 2θ (d = 7.1 Å), kaolinite at 24.8° 2θ (d = 3.59 Å), chlorite at 25.1° 2θ (d = 3.54 Å), quartz at 26.6° 2θ (d = 3.4 Å), feldspar including both plagioclase and K-feldspar at 27.7° 2θ (d = 3.2 Å), calcite at 29.4° 2θ (d = 3.0 Å), and dolomite at 30.9° 2θ (d = 2.9 Å) were determined based on the peak identification protocols of Biscaye (1965) and Elvelhøi and Rønningsland (1978).

3. Results

3.1. Surface sediments

3.1.1. Sediment color

The brightness L* was higher (brighter) in the Bering Sea and decreased northwards in the western Arctic Ocean (Fig. 2). In the western Arctic Ocean north of 75°N, L* was high on the Arlis Plateau and decreased eastwards to the Northwind Plateau (Fig. 2). The red−green contrast a* was higher (more reddish) in the western Arctic Ocean north of 75°N than in the Chukchi and Bering seas (Fig. 2). The yellow−blue contrast b* was high (yellowish) in the western Arctic Ocean north of 75°N and decreased southwards in the Chukchi Sea to the Bering Sea (Fig. 2). The b* value was lowest in the Yukon Estuary.

In the western Arctic Ocean, L* tended to decrease with increasing water depth to 600 m, and a* and b* tended to increase (Fig. 3). Below 600 m, these color indices were nearly constant, except for some western Arctic sediment around 1200 m that showed a higher L* (Fig. 3). In the Bering Sea, the L* and a* values of the slope sediments around 1000 and 2500 m were no different to those of the shelf sediments, and the b* values of the slope sediments corresponded to the values obtained from the outer shelf sediments (Fig. 3).

3.1.2. Minerals

Quartz, feldspar including plagioclase and K-feldspar, illite including mica, chlorite, kaolinite, hornblende, calcite, and dolomite were detected in the study samples (Fig. 4). Chlorite at 3.54 Å and kaolinite at 3.59 Å could be quantified separately in 46 of the 57 samples. The diffraction intensity of chlorite + kaolinite at 7.1 Å was significantly positively correlated with that of chlorite at 3.54 Å (r = 0.89), but not with that of kaolinite at 3.59 Å (r = 0.39; Fig. 5). This indicates that the diffraction intensity of chlorite + kaolinite is governed mainly by the amount of chlorite in the study area. Plagioclase ranged from anorthite to albite. Quartz and feldspar were most abundant in the northern Bering Sea, and their abundance decreased northwards in the shelf area of the Chukchi Sea to the western Arctic Ocean north of 75°N (Fig. 4). Smear-slide observations showed that quartz and feldspar are the major constituents of the sand and silt. Illite, chlorite + kaolinite, and chlorite were abundant in the western Arctic Ocean north of 75°N and the Mackenzie River estuary, but decreased in abundance southwards from the Chukchi Sea to the Being Sea (Fig. 4). The areas with high illite, chlorite + kaolinite, and chlorite contents correspond to the areas dominated by fine sediments (Fig. 3 in Park et al., 2014, Fig. 4). Kaolinite was abundant in the Northwind Ridge and Mackenzie Delta areas and abundantly found in one sample from the Yukon River estuary (Fig. 4). Hornblende was abundant in the Bering Sea, in particular in the Yukon River estuary, but its abundance declined northwards in the Chukchi Sea (Fig. 4). Calcite was abundant in the western Arctic Ocean north of 75°N, but was below the detection limit in other areas. Smear-slide observations showed that calcite is a constituent of the foraminifera and detrital grains. Dolomite was
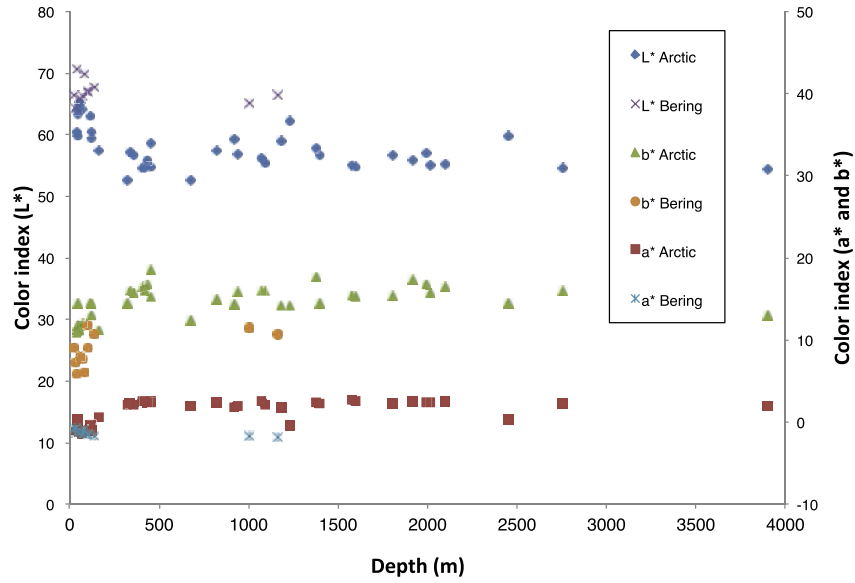
Fig. 3. Depth plots of L*, a*, and b* for the western Arctic Ocean and Bering Sea sediments.
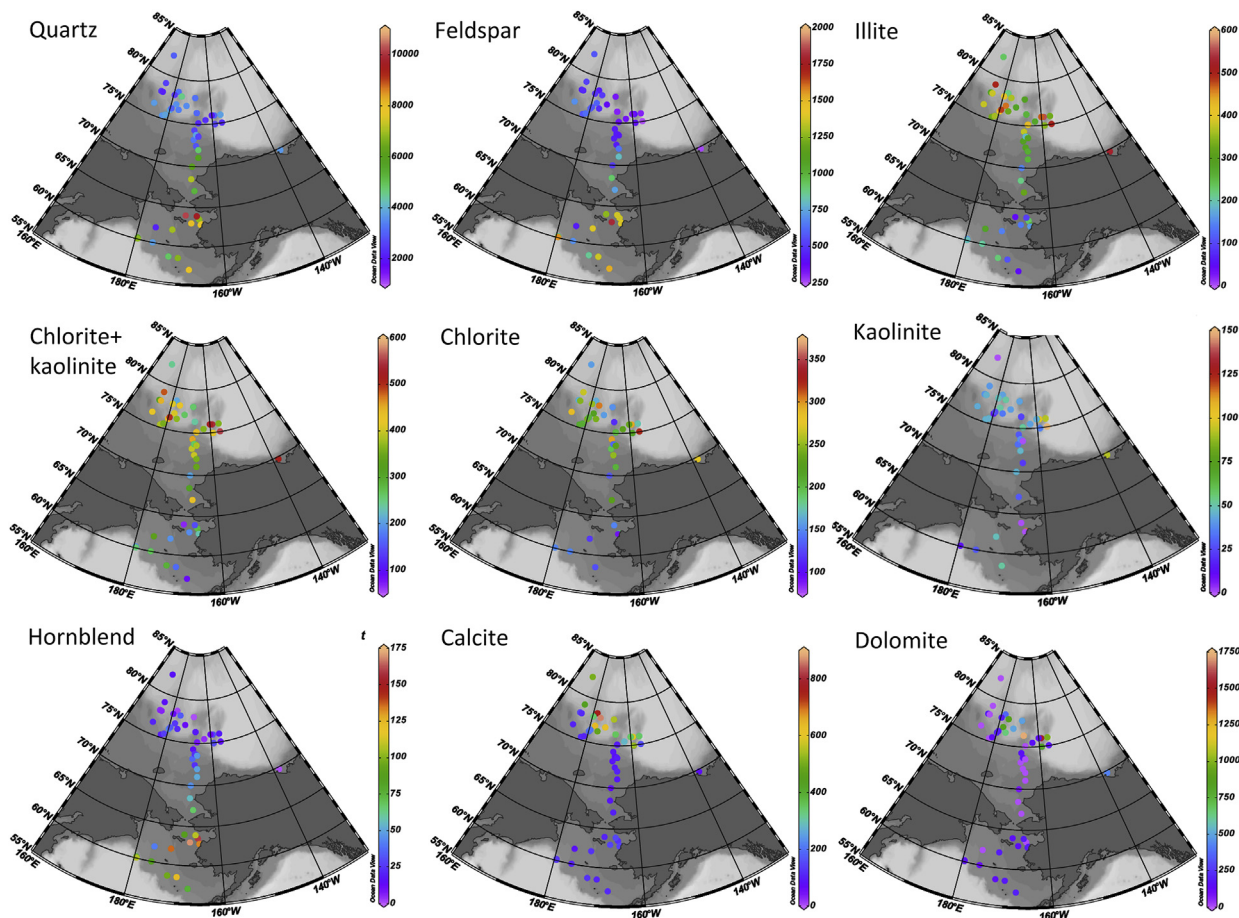
Fig. 4. Spatial distributions of the diffraction intensities of quartz, feldspar, illite, chlorite + kaolinite, chlorite, kaolinite, hornblende, calcite, and dolomite for the surface sediments.

detected but became lower in abundance westwards in the western Arctic Ocean north of 75°N (Fig. 4). Dolomite was below the detection limit in the other areas (Fig. 4). Smear-slide observation showed that dolomite is a constituent of the detrital grains.

3.2. Cores

3.2.1. Sediment color

In all five short cores, L* was lower (darker), a* was higher (more

Fig. 5. Plots of the diffraction intensities of (A) chlorite at 3.54 Å and (B) kaolinite at 3.59 Å against the diffraction intensity of chlorite + kaolinite at 7.14 Å.
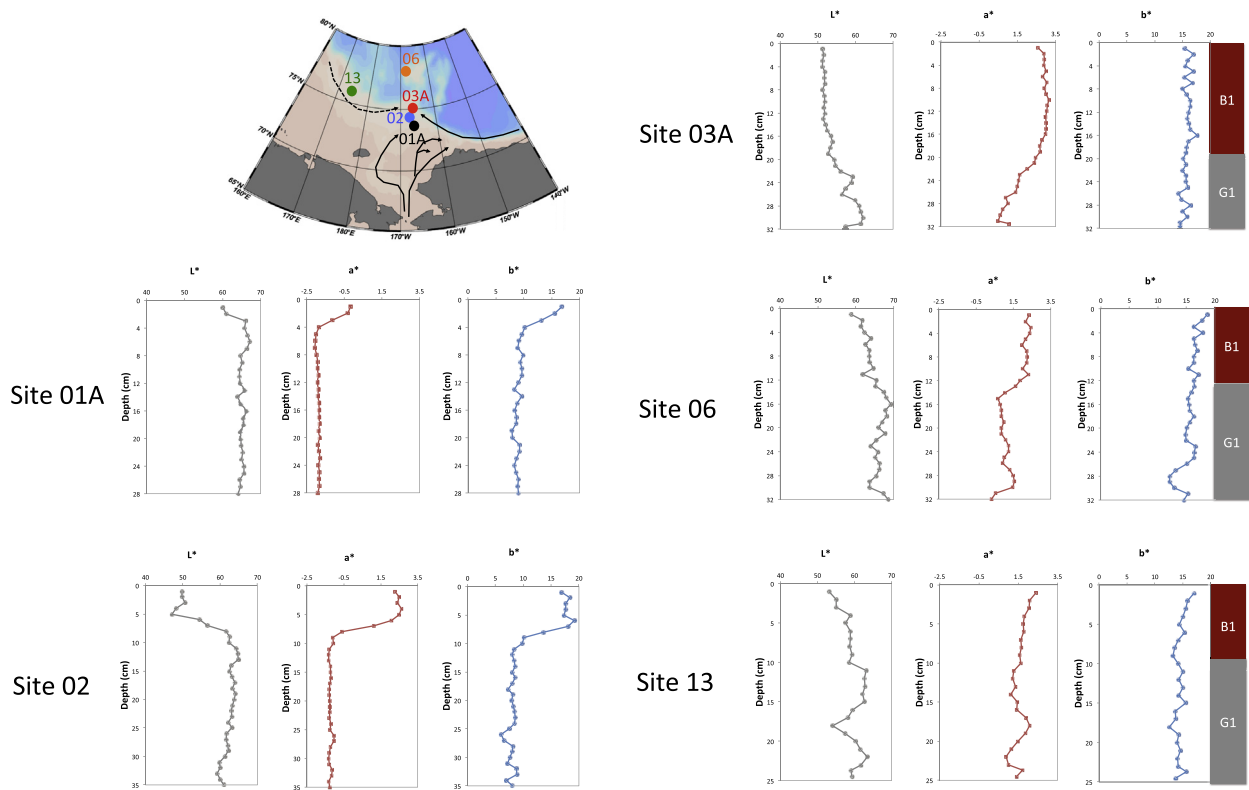
Fig. 6. Vertical profiles of color indices L*, a*, and b* in cores 01A MUC, 02 MUC, 03A MUC, 06 MUC, and 13 MUC. Map indicates the locations of cores and currents.

reddish), and b* was higher (more yellowish) in the upper horizon than in the lower horizon (Fig. 6). The color change occurred at a depth of 2–3 cm in core 01A MUC, 6–7 cm in core 02 MUC, 19–23 cm in core 03A MUC, 12–15 cm in core 06 MUC, and 11 cm in core 13 MUC (Fig. 6). The age–depth model of core ARA02B 01A GC retrieved at the same site as core 01A MUC indicated that the study interval (0–35 cm) covers the last 600 years (Masanobu Yamamoto and Song-Il Nam, unpublished data). Therefore, the study interval corresponds to the late Holocene. The lithology of core 02 MUC is similar to core 01A MUC, suggesting that the study interval (0–35 cm) was also deposited during the Holocene. The color boundaries in these two cores do not correspond to lithological

boundaries, but reflect the redox boundary between the oxic layer [Fe(III) state] in the upper horizon and the anoxic layer [Fe(II) state] in the lower horizon, as is often seen in sediments in other oceans (Nagao and Nakashima, 1991). In contrast, the color changes in cores 03A MUC and 06 MUC *did* correspond to the lithological boundaries. The sediments of the upper horizon consisted of clayey silt, whereas the sediments of the lower horizon consisted of silt with ice-rafted debris. The upper brownish layer was assigned to the Holocene B1 layer, and the lower grayish layer was assigned to the last glacial G1 layer, which is an established stratigraphy in the offshore area of the western Arctic Ocean (Polyak et al., 2004). The boundary between the B1 and G1 layers has been dated to 12.5 ka
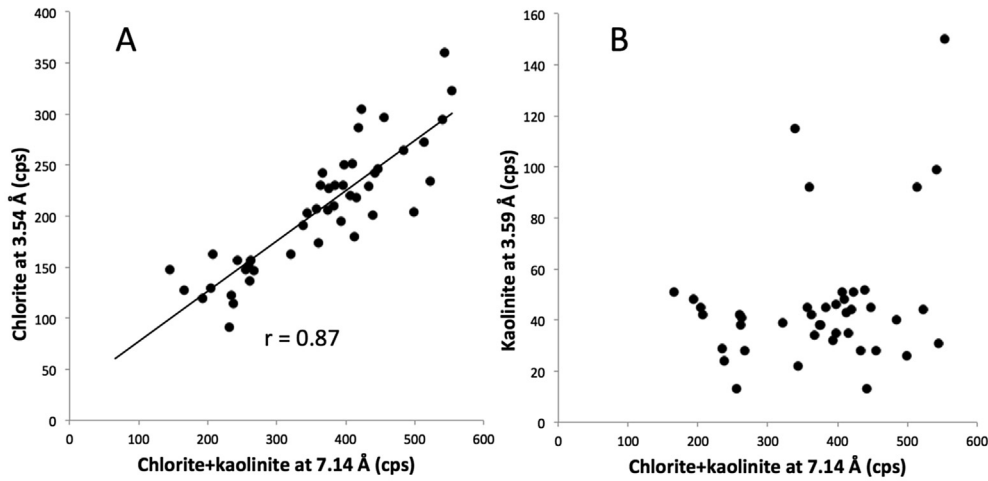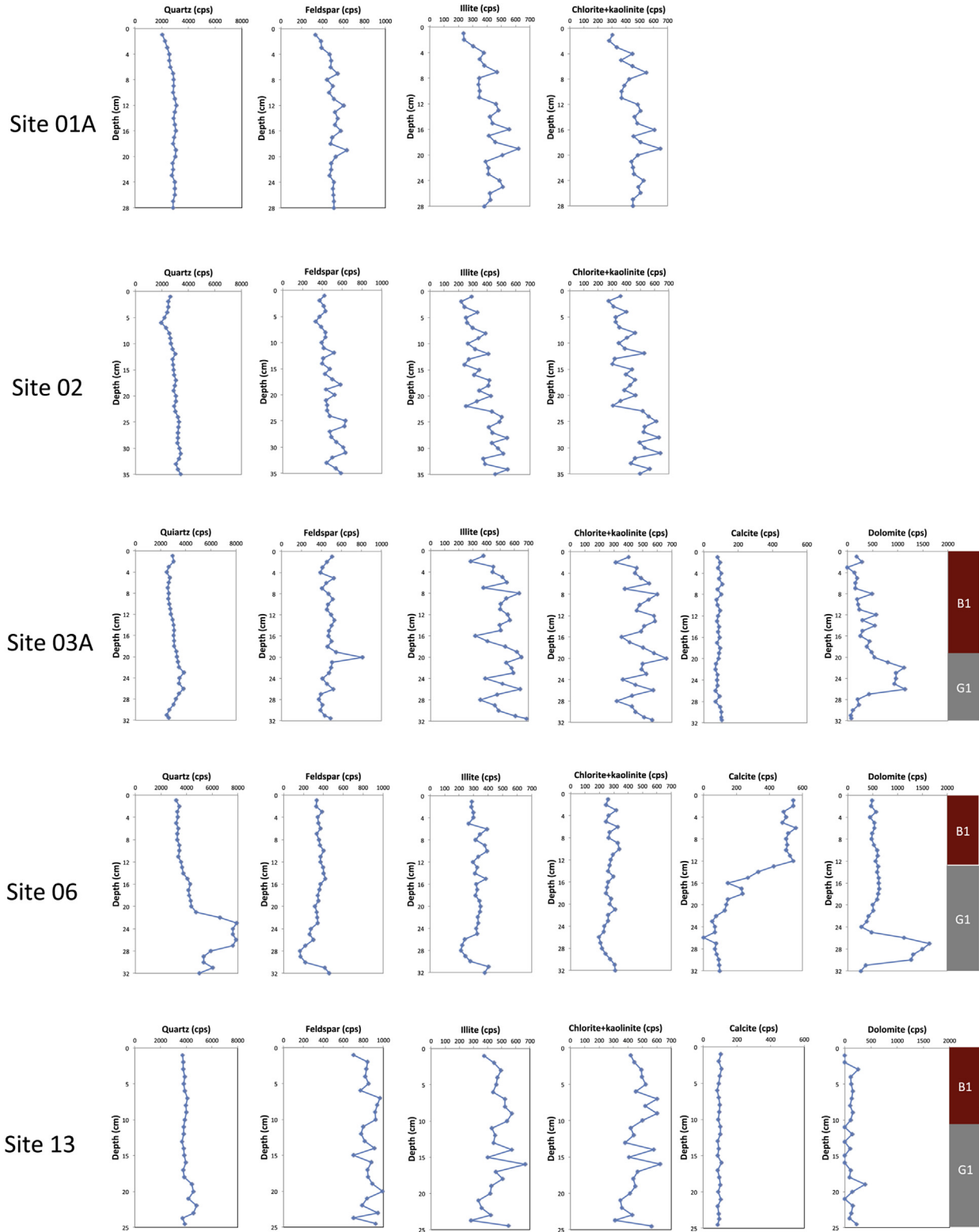
Fig. 7. Vertical profiles of the diffraction intensities of quartz, feldspar, illite, chlorite + kaolinite, calcite, and dolomite in cores 01A MUC, 02 MUC, 03A MUC, 06 MUC, and 13 MUC.

in core AR92-P25 on the Northwind Ridge (Polyak et al., 2009). The color changes in core 13 MUC do not correspond to the lithological boundaries. The sediments consist of silt throughout the entire core, but the color change is similar to that of core 06 MUC. By correlating the color indices, the upper brownish layer (0−11 cm) was tentatively assigned to the Holocene B1 layer, and the lower yellowish layer (11−24.5 cm) was assigned to the last glacial G1 layer.

Table 2
Correlation coefficients between color indices and sand, silt and clay contents in surface sediment samples.

Color	L*	a*	b*	Number of samples correlated
Water depth	−0.54	0.56	0.48	52
Sand (%)	0.80	−0.68	−0.87	40
Silt (%)	−0.72	0.56	0.81	40
Clay (%)	−0.84	0.88	0.83	40
Illite	−0.71	0.60	0.63	56
Hornblende	0.73	−0.63	−0.83	56
Chlorite + kaolinite	−0.63	0.47	0.58	56
Quartz	0.72	−0.55	−0.83	56
Feldspar	0.70	−0.57	−0.83	56
Calcite	−0.38	0.52	0.52	56
Dolomite	−0.35	0.49	0.38	56

Sand, silt and clay contents refer to Nagashima et al. (2012) and Park et al. (2014).

Table 3
Correlation coefficients between mineral intensities and sand, silt and clay contents in 40 surface sediment samples.

Intensity (cps)	Sand (%)	Silt (%)	Clay (%)
Quartz	0.90	−0.90	−0.66
Feldspar	0.91	−0.91	−0.68
Illite	−0.77	0.72	0.70
Chlorite + kaolinite	−0.77	0.76	0.60
Hornblende	0.84	−0.81	−0.70
Calcite	−0.36	0.27	0.56
Dolomite	−0.29	0.20	0.50

Sand, silt, and clay contents refer to Nagashima et al. (2012) and Park et al. (2014).

3.2.2. Minerals

Quartz, feldspar, illite, and chlorite + kaolinite were the major minerals detected in cores 01A MUC and 02 MUC. The abundances of these minerals increased gradually with increasing depth, but the relative abundances were almost constant (Fig. 7). In core 03A MUC, quartz, feldspar, illite, and chlorite + kaolinite were the major minerals in the B1 layer, and dolomite and quartz increased in the G1 layer (Fig. 7). In core 06 MUC, quartz, feldspar, illite, chlorite + kaolinite, calcite, and dolomite were the major minerals in the B1 layer, and dolomite and quartz increased while calcite decreased in the G1 layer (Fig. 7). In core 13 MUC, quartz, feldspar, illite, and chlorite + kaolinite were the major minerals in the B1 layer, and quartz increased in the G1 layer.

4. Discussion

4.1. Factors controlling sediment color

In the study area, the fine offshore sediments were dark brownish in color (lower L*, and higher a* and b*), whereas the coarse inner shelf sediments were a light olive-gray. In the Arctic Ocean, manganese oxide forms the dark-brown sediments of the deep basins (Jakobsson et al., 2000; Löwemark et al., 2013). The dissolution of manganese in shelf sediments and precipitation of manganese in deeper sediments are the major processes influencing color differences between shelf and deeper sediments in the western Arctic Ocean (Löwemark et al., 2013). In the Bering Sea, the slope sediments have the same L* values as the shelf sediments, which suggests that the dissolution and precipitation of manganese does not have a major influence on sediment color in this area.

L* has a positive correlation with sand content as well as with the XRD intensities of quartz and feldspar, but a negative correlation with the XRD intensities of illite and chlorite + kaolinite (Table 2). Quartz and feldspar are more abundant, and clay minerals are less abundant, in sand than in clay (Table 3). As quartz and feldspar have a higher reflectance than clay minerals, the higher abundance of quartz and feldspar contributes to the higher L* in the coarse shallower sediments.

The a*−b* diagram shows differences in the color indices between the Arctic inner shelf and basin surface sediments (Fig. 8A). It also shows that the Bering sediments have a lower a* (more greenish) and b* (more bluish) values than the Arctic sediments (Fig. 8). This difference seems to correspond to the rate of primary production in these areas; sediments with lower a* and b* values were sampled from the areas of higher productivity (Springer et al., 1996), and this can be attributed to the formation of bluish-greenish Fe(II) in the more reducing sedimentary environments generated by the high organic influx. On the a*−b* diagram, all of the Arctic cores show a decreasing trend in a* and b* with increasing sediment depth, but the decrease in a* is smaller in cores 03A MUC, 06 MUC, and 13 MUC than in cores 01A MUC and 02 MUC (Fig. 8B). We identified the deeper grayish layers of the former cores as the G1 layer that was deposited during the last glacial period (Polyak et al., 2004), whereas the deeper grayish layers of the latter cores consist of Holocene sediments and were identified as reducing layers. This diagram is useful to distinguish the origin of the grayish layers.

Based on these results, we infer that the sediment color in the Arctic samples studied here is governed by water depth, diagenesis, and mineral composition. The a*−b* diagram is useful for tracing the color change during diagenesis in these Arctic sediments.

4.2. Sources of quartz, feldspar, and hornblende

Quartz and feldspar were most abundant in the northern Bering Sea and their abundance decreased northwards across the Chukchi shelf to the western Arctic Ocean north of 75°N (Fig. 4). This trend is consistent with that of grain size (Fig. 3 in Park et al., 2014). The intensities of quartz and feldspar are positively correlated with sand content (Table 3). This is consistent with a smear-slide observation that both minerals are major constituents of sand. Park et al. (2014) showed that coarse sediments are distributed in the Yukon and Mackenzie River estuaries, the northern Bering Sea near the Bering Strait, and some areas of the Bering Sea. They attribute the dominance of coarse sediments in the inner shelf of the Chukchi and Bering seas to a combination of coastal erosion, river discharge from small Alaskan and Siberian rivers and the Yukon River, and the selective removal of fine particles in high-energy environments. The riverine discharge of sand grains and the selective removal of finer grains by re-suspension in the shelf areas of the Chukchi and Bering seas account for the high abundances of quartz and feldspar on the inner shelf of the Chukchi and Bering seas.

In the area north of 75°N, the feldspar/quartz ratio is higher in the western areas, such as the East Siberian slope, the Arlis Plateau, and the Makarov basin, than in the eastern areas such as the Chukchi Abyssal Plain, the Chukchi Plateau, the Northwind Abyssal Plain, and the Northwind Ridge (Fig. 9). This zonal gradient of the feldspar/quartz ratio suggests that feldspar-rich sediments are derived from the Siberian margin by the slope current that flows east along the East Siberian slope, as was recently suggested by a mooring observation on the East Siberian slope (Koji Shimada, unpublished data), whereas quartz-rich sediments are derived from the North American margin by the BG circulation (Vogt, 1997; Stein, 2008; Darby et al., 2011). The Laptev Sea sediments have a higher feldspar/quartz ratio than the sediments off the Canadian Arctic archipelago (Vogt, 1997). This suggests that the feldspar/quartz ratio can be used as a contribution index of East Siberian grains against North American grains.

Hornblende is abundant in the Bering Sea, particularly in the Yukon River estuary, but becomes less abundant northwards in the
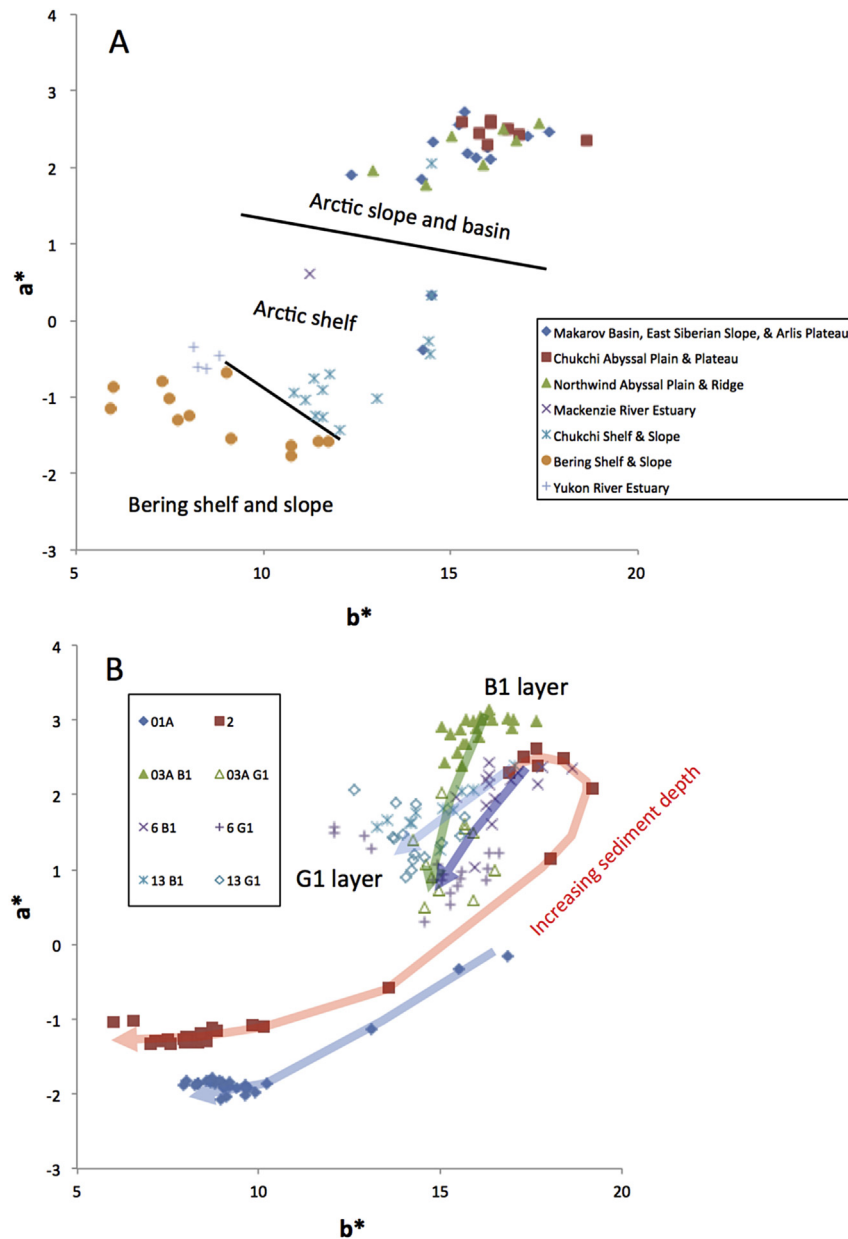
Fig. 8. (A) The a*–b* diagram showing western Arctic Ocean and Bering Sea surface sediments and (B) the down-core sediments from cores 01A MUC, 02 MUC, 03A MUC, 06 MUC, and 13 MUC in the western Arctic Ocean.

Chukchi Sea (Fig. 4). The intensity of hornblende is correlated positively with sand content (Table 3). The distribution of hornblende suggests that it originated from intermediate igneous rocks and/or metamorphic rocks in the Yukon River drainage basin (Beikman, 1980; Brabets et al., 2000).

A high feldspar/quartz ratio is associated with a high intensity of hornblende in the Bering Sea (Figs. 4 and 9). This association suggests that the detrital matter is derived from intermediate igneous rocks and/or metamorphic rocks. The restricted distribution of feldspar and hornblende-rich sediments suggests that the Yukon River discharge contributes to the supply of feldspar and hornblende.

4.3. Sources of illite, chlorite, and kaolinite

Illite and chlorite + kaolinite are abundant in the western Arctic Ocean north of 75°N and the Mackenzie River estuary, but their abundance decreases southwards across the Chukchi shelf to the Bering Sea (Fig. 4). The intensities of illite and chlorite + kaolinite are correlated positively with silt and clay contents (Table 3), reflecting that both illite and chlorite are constituents of the finer-grained material.

Illite is generally the most abundant clay mineral in marine sediments, and this can be explained by the high concentration of micas in many rock types, the widespread abundance of illite in many soils, and its relative resistance to chemical weathering (Biscaye, 1965). Illite commonly occurs in Arctic shelf sediments, and is the most abundant clay mineral on both the Alaskan and East Siberian margins (Naidu and Mowatt, 1983; Vogt, 1997; Kalinenko, 2001; Stein, 2008). Illite is the most abundant clay in the fluvial bed load of Alaskan and East Siberian rivers (Naidu et al., 1982; Naidu and Mowatt, 1983), which contributes to the ubiquitous distribution of illite in the study area.

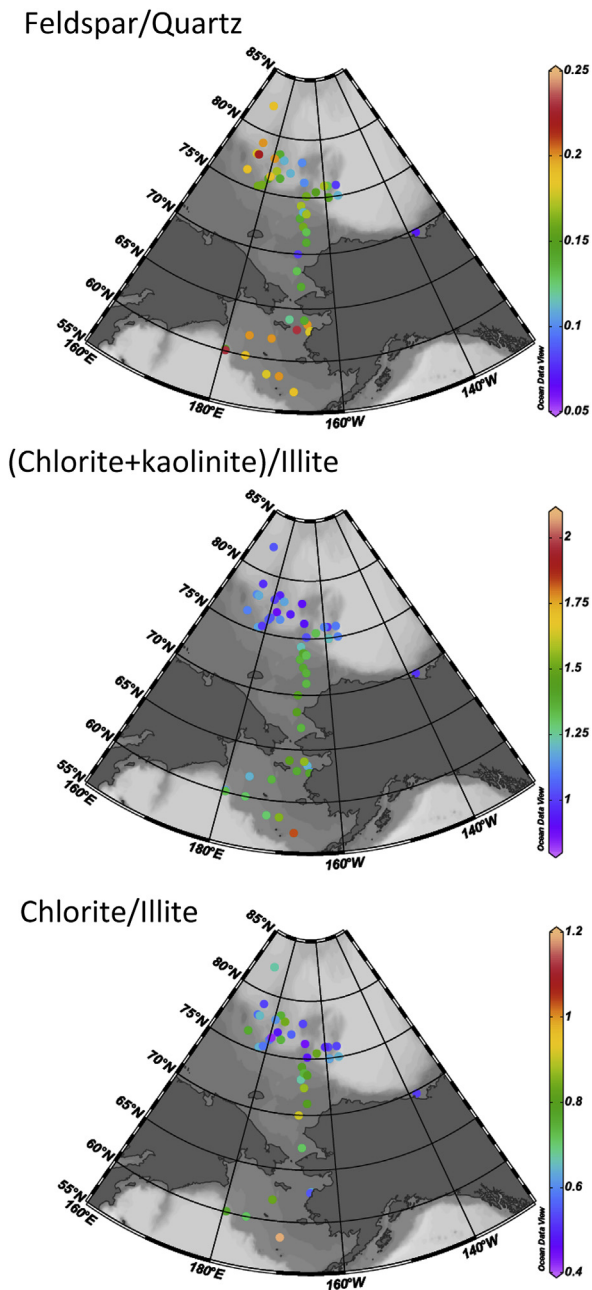Chlorite is more prevalent in soil at higher latitudes, where

Feldspar/Quartz

(Chlorite+kaolinite)/Illite

Chlorite/Illite

Fig. 9. Spatial distributions of the diffraction intensity ratios of feldspar to quartz, and of chlorite + kaolinite and chlorite to illite.

chemical weathering is less intense, and is a major component of fresh glacial rock flour derived from basic rocks (Biscaye, 1965). Chlorite occurs abundantly near the coasts of Alaska, Canada, and the Aluetians (Griffin and Goldberg, 1963). The published chlorite abundance in the bed load from 10 Alaskan rivers and an East Siberian river shows that the rivers of western and southern Alaska contain more chlorite than those of northern Alaska and Canada (Fig. 10; Naidu and Mowatt, 1983), and this reflects the geology of the drainage basins, which are underlain in large part by basic rocks. Kalinenko (2001) suggested that chlorite grains are more mobile than illite grains under conditions of intense hydrodynamic activity. Consequently, chlorite grains can be transported the long distance from the northern Bering Sea to the Chukchi Sea.

The (chlorite + kaolinite)/illite and chlorite/illite ratios were

high in the Bering Sea and decreased northwards from the Chukchi shelf to the western Arctic Ocean north of 75°N (Fig. 9). Previous studies indicated that illite is common in the Arctic Ocean, whereas chlorite is more abundant in the Bering Sea (Kalinenko, 2001). The chlorite/illite ratio was higher in the bed load of rivers and deltaic sediments from western Alaska than from other regions, and the value decreased northwards from the Yukon River in southwestern Alaska to the Canning River on the North Slope of Alaska (Fig. 10; Naidu and Mowatt, 1983). Naidu and Mowatt (1983) suggested that clay minerals delivered by the Yukon and Kuskokwim rivers in western Alaska enter Chukchi Sea sediments via the Bering Strait. Based on the distribution of chlorite in the Chukchi Sea, Kalinenko (2001) suggested that chlorite grains are transported from the Bering Sea to the Chukchi Sea via the Bering Strait. Ortiz et al. (2009) used chlorite abundance in a northern Chukchi Sea core as a tracer of Pacific water. Our results are consistent with the observations of these previous studies and suggest that the (chlorite + kaolinite)/illite ratio is a useful contribution index for the Bering Strait inflow.

Kaolinite, which is found in soils that have formed from the chemical weathering of rocks in hot, moist climates (Biscaye, 1965), is abundant in the Northwind Ridge and Mackenzie Delta areas where the BG circulation exerts an influence (Fig. 4). As the study area is situated in a polar region where kaolinite formation in soils is negligible, the kaolinite here must originate from the erosion of outcrops of kaolinite-rich rocks. The kaolinite/illite ratio was higher in the bed load of rivers and deltaic sediments from the North Slope of Alaska and Canada (Fig. 10; Naidu and Mowatt, 1983). This suggests that kaolinite in the Northwind Ridge originated from ancient rocks exposed on the North Slope and was delivered by water or sea ice via the Beaufort Gyre circulation.

4.4. Source of dolomite

Dolomite was detected on the Northwind Ridge and the Chukchi Plateau (Fig. 4). Dolomite is exposed in the Canadian Arctic Archipelago and is abundant in glacial till on the southwestern Canadian Archipelago (Bischof et al., 1996). The dolomite debris in the western Arctic sediments is most probably delivered by icebergs via the BG circulation from the Canadian Arctic Archipelago (Bischof et al., 1996; Bischof and Darby, 1997; Phillips and Grantz, 2001). Dolomite was below the detection limit in the samples obtained from the shelf areas of the Chukchi and Bering seas in the present study. There is no significant source of dolomite grains in this area (Beikman, 1980).

4.5. The feldspar/quartz and (chlorite + kaolinite)/illite diagram

All of the surface sediment samples are plotted in the diagram of the feldspar/quartz against (chlorite + kaolinite)/illite ratios (Fig. 11). The samples from the western Arctic Ocean north of 75°N plot in the upper half of the diagram; those from the eastern areas, such as the Northwind Ridge and the Chukchi Plateau, plot on the right side; and those from the western area, that is, the Arlis Plateau, plot to the left. The Chukchi and Bering Sea samples plot in the lower half. This diagram aids our understanding of the provenance of the sediments in the western Arctic Ocean and helps us to evaluate the influence of the Bering Strait inflow and the BG circulation.

4.6. Provenance of the western Arctic sediments during the last glacial period

The mineral composition of the short cores from the Chukchi Plateau, the Chukchi shelf, and the East Siberian slope revealed the
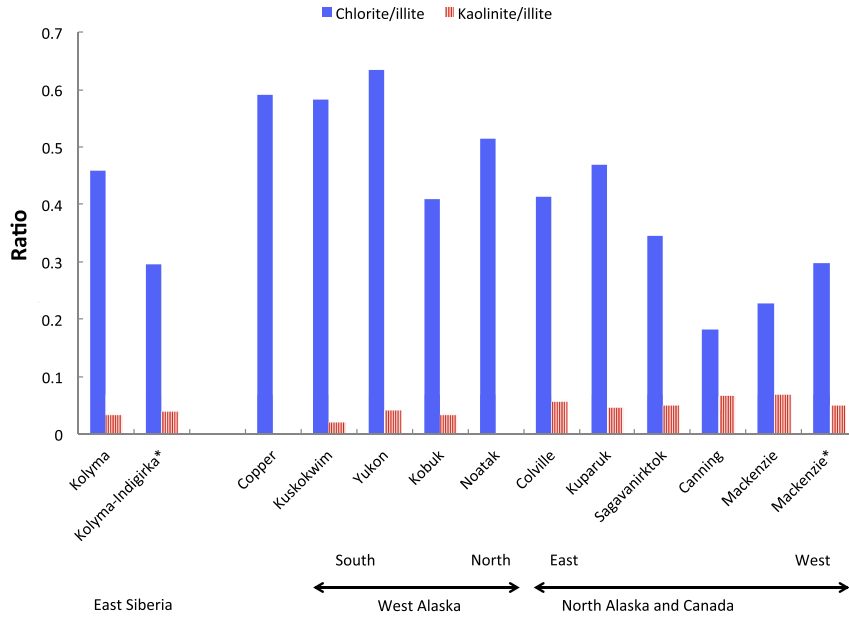
Fig. 10. The chlorite/illite and kaolinite/illite ratios in the bed loads of Alaskan and East Siberian rivers and deltaic sediments (*) (after Naidu and Mowatt, 1983).
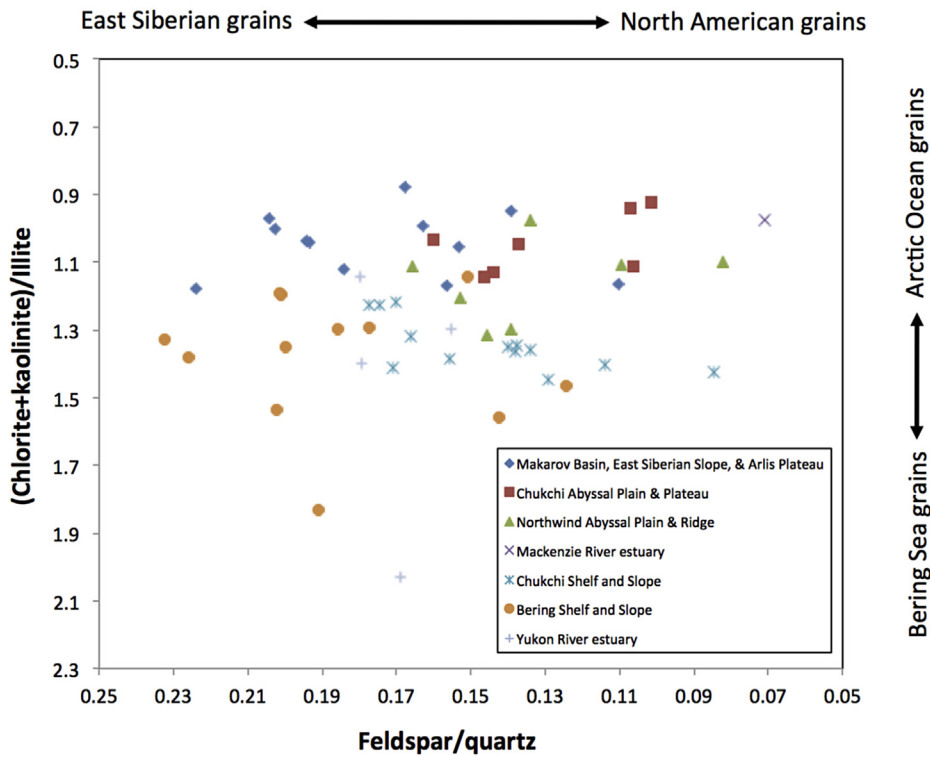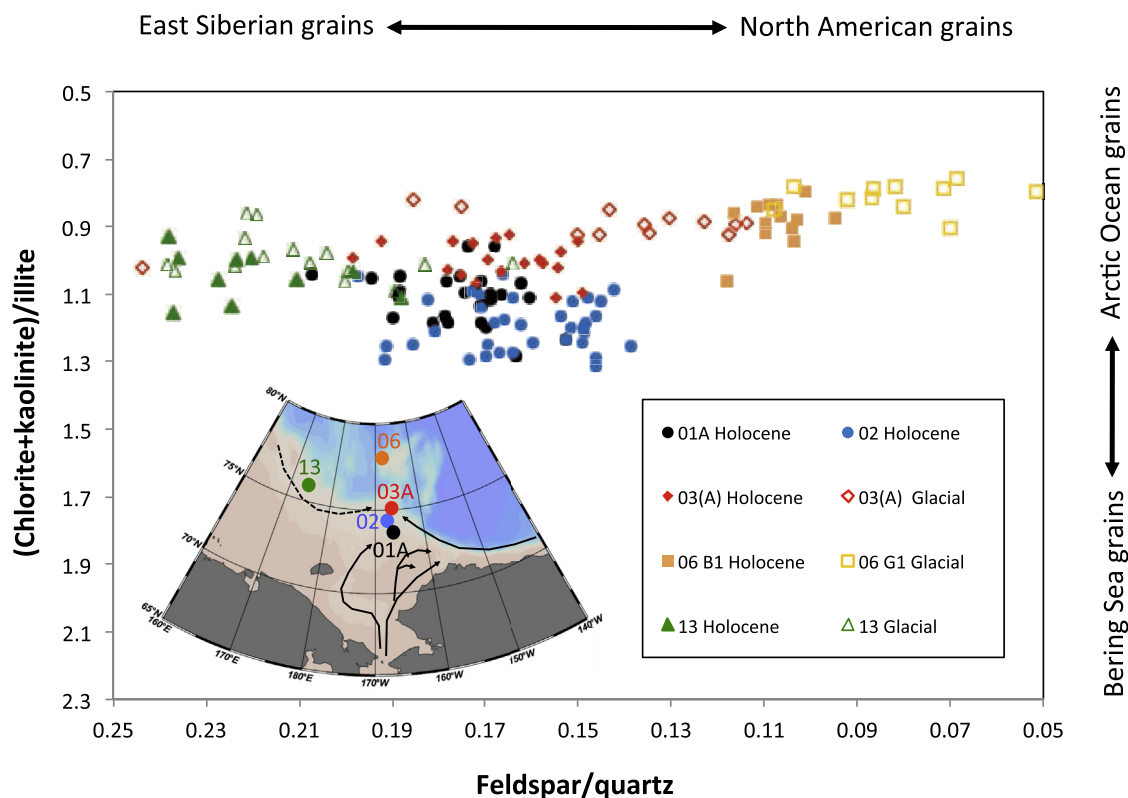

Fig. 11. Mineral composition of surface sediments on the plot of the feldspar/quartz against (chlorite + kaolinite)/illite ratios.

provenance of the sediments deposited since the last glacial period. All of the samples have a low (chlorite + kaolinite)/illite ratio (Fig. 12). This indicates that the contribution of the Bering Strait inflow was negligible in both the last glacial and Holocene periods in the study area. In cores 01A MUC and 02 MUC from the Chukchi Sea, Holocene sediments plot in relatively small areas, indicating that the depositional environments remained unchanged over the period of deposition (Fig. 12). On the other hand, in cores 03A MUC

and 06 MUC from the Chukchi Plateau, and core 13 MUC on the slope of the East Siberian Sea, the sediments showed a relatively large fluctuation in the feldspar/quartz ratio, suggesting that the relative intensities of the subsurface slope current that flows east along the Siberian margin, and also of the BG circulation, changed significantly during the depositional period (Fig. 12).

The abundance peaks of quartz and dolomite in the G1 layer can be correlated among cores 03A MUC, 06 MUC, and 13 MUC (Fig. 7).

Fig. 12. Mineral composition of Holocene and the last glacial sediments in cores 01A, 02, 03A MUC, 06 MUC, and 13 MUC on the plot of the feldspar/quartz against (chlorite + kaolinite)/illite ratios. Map indicates the locations of cores and currents.

The peaks are most enhanced in core 06 MUC. This probably indicates that the site of core 06 MUC was more influenced by iceberg discharge because it was located closer to the main path of icebergs during the last glacial episode (Bischof and Darby, 1997).

A high abundance of calcite was seen in the B1 layer of Core 06 MUC (78°N, 453 m water depth), but not in cores 03A MUC (75°N, 423 m) and 13 MUC (75°N, 340 m). In the surface sediments, calcite abundance depends on the latitude and water depth, and calcite abundance was nearly below the detection limit in the sediments sampled from latitudes <76°N and water depths <400 m in the study area (Fig. 4). Previous observations have indicated the presence of corrosive water centered at 100 m on the shelf and slope (<76°N) in the Chukchi Sea and Chukchi Borderland areas (Steinacher et al., 2009). Cores 03A MUC and 13 MUC were recovered from areas covered by this corrosive water; consequently, these sediments might have been affected by carbonate dissolution.

5. Conclusions

The diagram of a* and b* is useful tool for tracing the color change in Arctic Ocean sediments during diagenesis. The zonal gradient of the feldspar/quartz ratio in the western Arctic Ocean suggests that the feldspar/quartz ratio can be used as a contribution index of East Siberian grains against North American grains. We found that the (chlorite + kaolinite)/illite ratio and the chlorite/illite ratios were high in the Bering Sea but decreased northwards in the Chukchi Sea. This suggests that the (chlorite + kaolinite)/illite and chlorite/illite ratios could be useful as an index of the contribution of the Bering Strait inflow. The diagram of the feldspar/quartz against (chlorite + kaolinite)/illite ratios aids our understanding of the provenance of the western Arctic Ocean sediments. At the Chukchi Plateau sites, sediments deposited during the last glacial period have lower feldspar/quartz ratios and a higher dolomite intensity than do the Holocene sediments. This implies that the contribution of North American grains was greater on the Chukchi Plateau, and iceberg discharge was more important in sediment transport over the last glacial period than during the Holocene.

References

Asahara, Y., Takeuchi, F., Nagashima, K., Harada, N., Yamamoto, K., Oguri, K., Tadai, O., 2012. Provenance of terrigenous detritus of the surface sediments in the Bering and Chukchi Seas as derived from Sr and Nd isotopes: implications for recent climate change in the Arctic regions. Deep-Sea Res. II 61—64, 155—171.

Beikman, H.M., 1980. Geologic Map of Alaska. Scale 1:2,500,000. U.S. Geological Survey, Washington, D.C.

Biscaye, P.E., 1965. Mineralogy and sedimentation of recent deep-sea clay in the Atlantic Ocean and adjacent seas and oceans. Geol. Soc. Am. Bull. 76, 803—832.

Bischof, J., Clark, D.L., Vincent, J.S., 1996. Origin of ice rafted debris: Pleistocene paleoceanography in the western Arctic Ocean. Paleoceanography 11, 743—756.

Bischof, J., Darby, D.A., 1997. Mid- to late Pleistocene ice drift in the western Arctic

Ocean: evidence for a different circulation in the past. Science 277, 74—78.

Brabets, T.P., Wang, B., Meade, R.H., 2000. Environmental and Hydrologic Overview of the Yukon River Basin, Alaska and Canada. U. S. Geological Survey Water-Resources Investigations Report 99—4204.

Darby, D.A., Bischof, J.F., 2002. Arctic ice export events and their potential impact on global climate during the late Pleistocene. Paleoceanography 17, 1025. http://dx.doi.org/10.1029/2001PA000639.

Darby, D.A., Bischof, J.F., 2004. A Holocene record of changing Arctic Ocean ice drift analogous to the effects of the Arctic Oscillation. Paleoceanography 19, PA1027. http://dx.doi.org/10.1029/2003PA000961.

Darby, D.A., Myers, W.B., Jakobsson, M., Rigor, I., 2011. Modern dirty sea ice characteristics and sources: the role of anchor ice. J. Geophys. Res. 116 (C09008), 1—18.

Darby, D.A., Ortiz, J.D., Grosch, C.E., Lund, S.P., 2012. 1,500-year cycle in the Arctic oscillation identified in Holocene Arctic sea-ice drift. Nat. Geosci. 5, 897—900.

Elvelhøi, A., Rønningsland, T.M., 1978. Semiquantitative calculation of the relative amounts of kaolinite and chlorite by X-ray diffraction. Mar. Geol. 27, M19—M23.

Griffin, G.M., Goldberg, E.D., 1963. Clay mineral distributions in the Pacific ocean. In: Hill, M.N. (Ed.), The Sea, III. Interscience Pub, New York, pp. 728—741.

Jakobsson, M., Løvlie, R., Al-Hanbali, H., Arnold, E., Backman, J., Mörth, M., 2000. Manganese and color cycles in Arctic Ocean sediments constrain Pleistocene chronology. Geology 28, 23—26.

Kalinenko, V.V., 2001. Clay minerals in sediments of the Arctic seas. Lithol. Mineral Resour. 36, 362—372 (Translated from Litologiya I Poleznye Iskopaemye, 4, 418—429).

Löwemark, L., März, C., O'Regan, M., Gyllencreutz, R., 2013. Arctic Ocean Mn-stratigraphy: genesis, synthesis and inter-basin correlation. Quat. Sci. Rev. 92, 97—111.

Miller, G.H., Alley, E.B., Brigham-Grette, J., Fitzpatrick, J.J., Polyak, L., Serreze, M.C., White, J.W.C., 2010. Arctic amplification: can the past constrain the future? Quat. Sci. Rev. 29, 1779—1790.

Nagao, S., Nakashima, S., 1991. A convenient method of color measurement of marine sediments by colorimeter. Geochem. J. 25, 187—197.

Nagashima, K., Asahara, Y., Takeuchi, F., Harada, F., Toyoda, S., Tada, R., 2012. Contribution of detrital materials from the Yukon River to the continental shelf sediments of the Bering Sea based on the electron spin resonance signal intensity and crystallinity of quartz. Deep-Sea Res. II 61—64, 145—154.

Naidu, A.S., Creager, J.S., Mowatt, T.C., 1982. Clay mineral dispersal patterns in the north bering and Chukchi seas. Mar. Geol. 47, 1—15.

Naidu, A.S., Mowatt, T.C., 1983. Sources and dispersal patterns of clay minerals in surface sediments from the continental shelf areas off Alaska. Geol. Soc. Am. Bull. 94, 841—854.

Nwaodua, E., Ortiz, J.D., Griffith, E.M., 2014. Diffuse spectral reflectance of surficial sediments indicates sedimentary environments on the shelves of the Bering Sea and western Arctic. Mar. Geol. 355, 218—233.

Ortiz, J.D., Polyak, L., Grebmeier, J.M., Darby, D., Eberl, D.D., Naidu, S., Nof, D., 2009. Provenance of Holocene sediment on the Chukchi-Alaskan margin based on combined diffuse spectral reflectance and quantitative X-Ray diffraction analysis. Glob. Planet. Change 68, 73—84.

Park, Y.H., Yamamoto, M., Nam, S.I., Irino, T., Polyak, L., Harada, N., Nagashima, K., Khim, B.K., Chikita, K., Saitoh, S.I., 2014. Distribution, source and transportation of glycerol dialkyl glycerol tetraethers in surface sediments from the western Arctic Ocean and the northern Bering Sea. Mar. Chem. 165, 10—24.

Phillips, R.P., Grantz, A., 2001. Regional variations in provenance and abundance of ice-rafted clasts in Arctic Ocean sediments: implications for the configuration of late Quaternary oceanic and atmospheric circulation in the Arctic. Mar. Geol. 172, 91—115.

Polyak, L., Curry, W.B., Darby, D.A., Bischof, J., Cronin, T.M., 2004. Contrasting glacial/interglacial regimes in the western Arctic Ocean as exemplified by a sedimentary record from the Mendeleev Ridge. Palaeogeogr. Palaeoclimatol. Palaeoecol. 203, 73—93.

Polyak, L., Bischof, J., Ortiz, J.D., Darby, D.A., Channell, J.E.T., Xuan, C., Kaufman, D.S., Løvlie, R., Schneider, D.A., Eberl, D.D., Adler, R.E., Council, E.A., 2009. Late Pleistocene stratigraphy and sedimentation patterns in the western Arctic Ocean. Glob. Planet. Change 68, 5—17.

Proshutinsky, A.Y., Johnson, M.A., 1997. Two circulation regimes of the wind-driven Arctic Ocean. J. Geophys. Res. 102 (C6), 12493—12514.

Rigor, I.G., Wallace, J.M., Colony, R., 2002. Response of sea ice to the Arctic oscillation. J. Clim. 15, 2648—2663.

Screen, J.A., Simmonds, I., 2010. The central role of diminishing sea ice in recent Arctic temperature amplification. Nature 464, 1334—1337.

Springer, A.M., McRoy, C.P., Flint, M.V., 1996. The Bering Sea Green Belt: shelf-edge processes and ecosystem production. Fish. Oceanogr. 5, 205—223.

Stein, R., Grobe, H., Wahsner, M., 1994. Organic carbon, carbonate, and clay mineral distributions in eastern central Arctic Ocean surface sediments. Mar. Geol. 119, 269—285.

Stein, R., 2008. Developments in Marine Geology: Arctic Ocean Sediments: Processes, Proxies, and Paleoenvironment. Elsevier, Amsterdam, 592pp.

Stein, R., Matthiessen, J., Frank Niessen, F., 2010a. Re-coring at Ice Island T3 site of key core FL-224 (Nautilus Basin, Amerasian Arctic): sediment characteristics and stratigraphic framework. Polarforschung 79, 81—96.

Stein, R., Matthiessen, J., Niessen, F., Krylov, A., Nam, S.I., Bazhenova1, E., 2010b. Towards a better (litho-) stratigraphy and reconstruction of quaternary paleoenvironment in the Amerasian basin (Arctic Ocean). Polarforschung 79, 97—121.

Steinacher, M., Joos, F., Frölicher, T.L., Plattner, G.K., Doney, S.C., 2009. Imminent ocean acidification in the Arctic projected with the NCAR global coupled carbon cycle-climate model. Biogeosciences 6, 515—533.

Shimada, K., Kamoshida, T., Itoh, M., Nishino, S., Carmack, E., McLaughlin, F., Zimmermann, S., Proshutinsky, A., 2006. Pacific Ocean inflow: influence on catastrophic reduction of sea ice cover in the Arctic Ocean. Geophys. Res. Lett. 33, L08605. http://dx.doi.org/10.1029/2005GL025624.

Vogt, C., 1997. Regional and temporal variations of mineral assemblages in Arctic Ocean sediments as climatic indicator during glacial/interglacial changes. Rep. Polar Res. 251, 1—309.

Vogt, C., Knies, J., Spielhagen, R.F., Stein, R., 2001. Detailed mineralogical evidence for two nearly identical glacial/deglacial cycles and Atlantic water advection to the Arctic Ocean during the last 90,000 years. Glob. Planet. Change 31, 23—44.

Wahsner, M., Müller, C., Stein, R., Ivanov, G., Levitan, M., Shelekhova, E., Tarasov, G., 1999. Clay-mineral distribution in surface sediments of the Eurasian Arctic Ocean and continental margin as indicator for source areas and transport pathways — a synthesis. Boreas 28, 215—233.

Weingartner, T., Aagaard, K., Woodgate, R., Danielson, S., Sasaki, Y., Cavalieri, D., 2005. Circulation on the north central Chukchi Sea shelf. Deep-Sea Res. II 52, 3150—3174.

Woodgate, R.A., Aagaard, K., 2005. Revising the Bering Strait freshwater flux into the Arctic Ocean. Geophys. Res. Lett. 32, L02602. http://dx.doi.org/10.1029/2004GL021747.

Woodgate, R.A., Aagaard, K., Swift, J.H., Falkner, K.K., Smethie, W.M., 2005a. Pacific ventilation of the Arctic Ocean's lower halocline by upwelling and diapycnal mixing over the continental margin. Geophys. Res. Lett. 32, L18609. http://dx.doi.org/10.1029/2005GL023999.

Woodgate, R.A., Aagaard, K., Weingartner, T., 2005b. A year in the physical oceanography of the Chukchi Sea: moored measurements from autumn 1990—1991. Deep-Sea Res. II 52, 3116—3149.